Maize and sunflower biomass estimation in southwest France using high spatial and temporal resolution remote sensing data

Martin Claverie, Valérie Demarez, Benoît Duchemin, Olivier Hagolle, Danielle Ducrot, Claire Marais-Sicre, Jean-François Dejoux, Mireille Huc, P. Keravec, Pierre Béziat, et al.

Title

Maize and sunflower biomass estimation in southwest France using high spatial and temporal resolution remote sensing data

Authors

Claverie M. [a], Duchemin B. [a], Hagolle O. [a], Ducrot D. [a], Marais-Sicre C. [a], Dejoux J.F. [a], Huc M. [a], Keravec P. [a], Béziat P. [a], Fieuzal R. [a], Ceschia E. [a] and Dedieu G. [a], Demarez V. [a].

[a] CESBIO, Unité mixte CNES-CNRS-IRD-UPS, 18, avenue Edouard Belin, 31401 Toulouse Cedex 4, France.

Corresponding author

Martin Claverie
Centre d'Etudes Spatiales de la BIOsphère
Address: CESBIO, 18 Avenue Edouard Belin, 31401 Toulouse Cedex 4, FRANCE
Telephone: +33561558543
Fax: +33561558500
E-mail: martin.claverie@gmail.com

Abstract

The recent availability of high spatial and temporal resolution (HSTR) remote sensing data (Formosat-2, and future missions of Venμs and Sentinel-2) offers new opportunities for crop monitoring. In this context, we investigated the perspective offered by coupling a simple algorithm for yield estimate (SAFY) with the Formosat-2 data to estimate crop production over large areas. With a limited number of input parameters, the SAFY model enables the simulation of time series of green area index (GAI) and dry aboveground biomass (DAM). From 2006 to 2009, 95 Formosat-2 images (8 meters, 1 day revisit) were acquired for a 24×24 km² area southwest of Toulouse, France. This study focused on two summer crops: irrigated maize (*Zea mays*) and sunflower (*Helianthus annuus*). Green area index (GAI) time series were deduced from Formosat-2 NDVI time series and were used to calibrate six major parameters of the SAFY model. Four of those parameters (partition-to-leaf and senescence function parameters) were calibrated per crop type based on the very dense 2006 Formosat-2 data set. The retrieved values of these parameters were consistent with the in situ observations and a literature review. Two of the major parameters of the SAFY model (emergence day and effective light-use efficiency) were calibrated per field relative to crop management practices. The estimated effective light-use efficiency values highlighted the distinction between the C4 (maize) and C3 (sunflower) plants, and were linked to the reduction of the photosynthesis rate due to water stress. The model was able to reproduce a large set of GAI temporal shapes, which were related to various phenological behaviours and to crop type. The biomass was well estimated (relative

error of 28%), especially considering that biomass measurements were not used for the calibration. The grain yields were also simulated using harvest index coefficients and were compared with grain yield statistics from the French Agricultural Statistics for the department of Haute-Garonne. The inter-annual variation in the simulated grain yields of sunflower was consistent with the reported variation. For maize, significant discrepancies were observed with the reported statistics.

1. Introduction

Soil carbon sequestration has been identified by the Intergovernmental Panel on Climate Change as one of the options for the mitigation of greenhouse gases (Hutchinson et al. 2004). Agricultural lands cover approximately 35% of the land surfaces and through photosynthesis and biomass production, agriculture can act as carbon sinks (Ceschia et al. 2010, Kutsch et al. 2010). However, many factors impact photosynthesis, including crop type, crop management practices, soil properties and climate. Thus, crop production is highly variable in both space and time. This variability should be quantified to improve the management of agricultural lands and to refine regional carbon balance estimates.

Land surfaces have been studied for many years using remote sensing reflectances and vegetation indices (Baret and Guyot 1991, Asrar et al. 1994, Moulin et al. 1998, Bastiaanssen et al. 2000, Basso et al. 2001, Pinter et al. 2003, Faivre et al. 2004, Scotford and Miller 2005, Duchemin et al. 2008b). Crops fields of South-West of France are often of small size and they experience high temporal dynamics due to plant growth and management practices (soil tillage, sowing, irrigation and harvest). Remote sensing satellites providing high frequency observations at a high spatial resolution are thus well designed to monitor cropping systems. Until recently, high spatial and temporal resolutions have not been attainable because of technological limitations. Currently, the Formosat-2 Taiwanese satellite has the unique capability of taking daily images at 8 m spatial resolution with a constant viewing angle (Chern et al. 2006). The high temporal resolution of the monodirectional Formosat-2 data allows the acquisition of very accurate surface reflectances and vegetation indices time series (Hagolle et al. 2008, Hagolle et al. 2010).

Previously, only a small number of agro-meteorological studies have been performed using both high spatial and temporal resolution images with constant viewing angles such as Formosat-2 data. Duchemin et al. (2008b) have presented a preliminary evidence of the usefulness of such data for land use mapping and agricultural water management for wheat crops in Morocco. Numerous studies (Courault et al. 2008, Bsaibes et al. 2009, Hadria et al. 2010, Fieuzal et al. 2011) have shown its utility for capturing the spatiotemporal variability of two key biophysical variables: albedo and green leaf area index. Hadria et al. (2009) have demonstrated the convenience of this type of data for the detection of agricultural operations such as ploughing or irrigation at the beginning of the cropping season. In this study, we analysed the potential for the use of high spatial and temporal resolution images to provide regular estimates of crop production over large areas. We used Formosat-2 data in combination with a simple algorithm for yield estimate (SAFY, Duchemin et al. 2008a).

Crop models were originally designed to simulate crop growth on agricultural fields where soil, climate and agricultural practices were well known and spatially homogeneous. They have been used in a wide range of agro-environmental issues. However, the application of crop models over large areas is still challenging because the soil properties, the climatic variables and the agricultural practices are highly variable in space and time (Boote et al. 1996, Moulin et al. 1998, Faivre et al. 2004, de Wit et al. 2005). In confronting this challenge, we have distinguished three categories of crop models:

i) Complex models that simulate a large set of agro-environmental variables through the description of numerous coupled phenological and physiological processes, such as photosynthesis, respiration, evapotranspiration and nitrogen uptake (e.g., AFRCWHEAT2, CERES, Sirius, SUCROS2, STICS, SWHEAT, see Jamieson et al. 1998 and Brisson et al. 2003 for reviews). These models require a large number of parameters and input data. This information may be available during scientific experiments, or it may be available from some farmers at a local scale, but it is generally not available over large areas.

ii) In contrast, very simple models calculate biomass as an empirical sum of vegetation indices derived from remote sensing observations (Tucker and Sellers 1986, Dong et al. 2003, Wessels et al. 2006). These models are all based on the light-use efficiency (LUE) theory (Monteith 1977). These models are uncomplicated to parameterise over large areas using time series of remote sensing data with low spatial resolution data acquired at 10-day or monthly intervals. They provide estimates of net primary production for natural ecosystems such as forests (e.g., Dong et al. 2003) or grasslands (e.g., Tucker et al. 1983, Prince 1991, Wylie et al. 1991, Loseen et al. 1995). However, these models appear less suited for crop monitoring because they do not accurately account for crop type and management (Faivre et al. 2004).

iii) The third category of crop models gathers the descriptions of the main biophysical processes (biomass accumulation, leaf partition, leaf senescence,...) and empirical parameterisations. These models combine the LUE theory with a simulation of the successive plant phenological phases. This semi-empirical approach, in which the number of formalisms and parameters is limited, enables studies over larger areas. Maas (1993) has demonstrated the value of such a model for simulating time series of leaf area index and dry aboveground biomass for maize and wheat crops. Lobell et al. (2003) and Liu et al. (2010), who worked on the combination of such semi-empirical models and remote sensing data, have underlined the need for high temporal and spatial resolution satellite data to improve model predictions.

The SAFY model (Duchemin et al. 2008a) belongs to this third category of semi-empirical models. It was specifically designed for large-scale studies because it describes the main biophysical processes using climatic data. Previous studies have shown that the SAFY model, once calibrated with green leaf area index time series, resulted in accurate estimates of dry aboveground biomass for irrigated wheat cultivated in semi-arid regions (Duchemin et al. 2008b, Hadria et al. 2009, Fieuzal et al. 2011).

The objective of this study was to evaluate the coupling between high spatial and temporal resolutions remote sensing data with a simple crop model to estimate crop production at regional scale. An example is shown using Formosat-2 images combined with the SAFY model applied to sunflower (*Helianthus annuus*) and maize (*Zea mays*) in southwest France. The experiment was performed during four successive agricultural seasons (2006-2009) with a focus on maize and sunflower crops, which are the two dominant summer crops cultivated in the southwest of France. Time series of Formosat-2 observations were used to calibrate parameters of the SAFY model over a region covering approximately 600 km^2. Evaluation of the model used an in situ data set collected from 2006 to 2009 and regional grain yield statistics.

2. Material and methods

2.1. Study area

The study area is a 24 × 24 km^2 area located near Toulouse, in southwest France (1°10′ E, 43°27′ N, Fig. 1). The climate is temperate continental with hot (daily mean temperature approximately 22.5 °C) and dry (38 mm/month of rainfall) summers. Arable lands cover up to 60% of the study area, of which 40% is cultivated during summer, predominantly with irrigated maize (grain and silage) and sunflower crops. The southeastern and the western parts of the study area are hilly landscapes with small fields (approximately 10 ha); the centre of the study area, near the Garonne River, is nearly flat with larger fields (approximately 25 ha).

In the study area, maize fields are sown from mid-April to beginning of June, and last until September-October. Most of maize fields are irrigated during hottest month (July and August). Sunflower fields are sown from end of March to end of June and are mainly non-irrigated.

2.2. Field data

The study was performed during from 2006 to 2009 on maize and sunflower crops. Four types of in situ data were measured: the dry aboveground biomass (DAM), the green area index (GAI) and the fraction of absorbed photosynthetically active radiation (FAPAR). The DAM and the SLA were estimated with a destructive method. The GAI and the FAPAR were estimated from hemispherical photographs.

The main characteristics of the field measurements are shown in Fig. 1 and Table 1. Two protocols were used to collect the data:

(i) Transect sampling protocol: the measurements of DAM were performed from 2006 to 2008 along two transects crossing the field. This protocol was applied in two fields belonging to the CarboEurope-IP Regional experiment (Dolman et al. 2006). These two fields are hereafter referred to as “Lamothe” and “Auradé”. They belong to an experimental farm managed by the Purpan Engineering School and to a farmers association (http://www.agriculteurs-aurade.fr/). Thirty plants were harvested 6 to 9 times per growing season (Table 1). For each plant, leaf biomasses were measured independently and leaf areas were measured using a planimeter (Licor 3100 Lincoln Inc., Nebraska) in order to derive the specific leaf area (SLA).

(ii) Elementary sampling unit (ESU) protocol: the measurements of DAM, GAI and FAPAR were performed within a 20 m sided square area. Eleven fields located near the “Lamothe” farm were sampled (back squares in Fig. 1 and Table 1). These fields are hereafter referred to as the ESU fields. The locations of the ESUs were recorded with a GPS. GAI and FAPAR were measured in 2008 using digital hemispherical photographs (DHPs). Each ESU was sampled with 13 DHPs applying the VALERI spatial sampling protocol (http://w3.avignon.inra.fr/valeri). The in situ data were collected 7 to 10 times during the growing season yielding 23 GAI and FAPAR estimations for maize and 19 for sunflower (Table 1). The DAM was estimated from 10 plants collected near the ESUs in 2008 and 2009, leading to 14 DAM estimations for maize and 11 for sunflower. In 2009, only one biomass measurement was performed per ESU during the growing season.

The concept of green area index (GAI, Baret et al. 2010) corresponds to the photosynthetically active plant area without organ distinctions. It is related to FAPAR and can be derived from DHPs. In our study, the DHPs were taken with a Nikon CoolPix 8400 camera equipped with a FC-E8 fisheye lens. The camera was put at the top of a pole to keep the viewing direction (looking downward) and the canopy-to-sensor distance constant (~1.5m) throughout the growing season. This protocol allowed the reduction of errors in the directional gap fraction estimates and thus in the FAPAR and GAI estimates (Demarez et al. 2008). The DHP were processed using CAN-EYE V5 (http://www4.paca.inra.fr/can-eye), which provides estimates of the daily FAPAR and of the "effective" and "true" GAI (Demarez et al. 2008, Baret et al. 2010). In this study, we used the effective GAI ($GAI_{eff,CAN\text{-}EYE}$), which is highly correlated with remote sensing observations and the daily FAPAR ($FAPAR_{daily,CAN\text{-}EYE}$).

In addition to these measurements, several farmers provided grain yield estimates for maize (4 estimates) and sunflower (37 estimates) for 12 fields located near Lamothe and for 16 fields located near Auradé (blue disks in Fig. 1).

2.3. Meteorological data

Meteorological data were generated by the mesoscale atmospheric analysis system SAFRAN, which is operational at Météo-France (Durand et al. 1993). Among other variables, SAFRAN simulates air temperature at 2 m above the ground (Ta), incoming global radiation (Rg) and precipitation (P) based on a combination of measurements (weather stations) and modelling. The data are available every 6 hours over a grid with an 8 km spatial resolution (plus symbols in Fig. 1).

The SAFRAN meteorological variable data were processed to compute daily mean Ta and cumulated daily Rg and P for each Fomosat-2 pixel (8 meters) of the study area. The spatial oversampling was performed using a bilinear spatial interpolation.

The evaluation performed by Quintana-Segui et al. (2008) all over the France have shown that Rg (RRMSE = 60%) and Ta (RRMSE = 13%) are accurately estimated by SAFRAN, while the accuracy of P was found lower (RRMSE = 100%), especially in mountainous areas.

The analysis of the meteorological variables over the Formosat-2 footprint revealed differences between the years. The driest and hottest years were 2006 and 2009; the cumulated daily precipitation for the summer growing season, from DoY (day of year) 125 to 250, was 147 mm in 2006 and 152 mm in 2009, whereas it reached 248 mm in 2008 and 273 mm in 2007. The cumulated air temperature during the same period was approximately 2570 °C in 2006 and 2009 and approximately 2370 °C in 2007 and 2008.

2.4. Formosat-2 data

Formosat-2 is a high spatial (8 meters) and temporal (daily revisit time) resolution satellite with four spectral bands (488, 555, 650 and 830 nm) and a 24 km field of view (Chern et al. 2006). Formosat-2 takes images at a constant viewing angle. Ninety-Five images were taken of our study area from 2006 to 2009 (Fig. 2). In 2006, the images were scheduled at a high priority level with a nominal time step of 3 days. The 2006 data set contained 51 images, including 27 images that were almost totally cloud-free. After 2006, only images with a cloud cover less than 20% were purchased. Thus, 14 images were available in 2007, 11 images in 2008 and 19 in 2009. In 2008, no cloud-free images were available from February 11 to June 19.

All of the Formosat-2 images were pre-processed for geometric, radiometric and atmospheric corrections and the filtering of clouds and shadows (Hagolle et al. 2008, Hagolle et al. 2010). This processing resulted in surface reflectances images and associated cloud-masks. The absolute location accuracy was 0.4 pixels, i.e., 3.2 m (Baillarin et al. 2008), which is quite satisfactory with respect to both the field and ESU sizes.

2.5. Land cover

Maize and sunflower were identified using classification and segmentation methods applied to Formosat-2 surface reflectances images. This processing was performed each year using all images acquired from January to December. The classification method was performed using a fuzzy contextual algorithm of the Iterative Conditional Mode type based on a Markovian model (Idbraim et al. 2009). The segmentation algorithm was based on a watershed method (Fjortoft et al. 1999) and leaded to homogenous units (called HU hereafter), corresponding to homogenous radiometric zones. The parameters used for the segmentation were chosen such that the agricultural fields were split in the case of high intra-field variability. As a result, an agricultural field corresponded to one or several HU (see Fig. 3). Only HU larger than 640 m^2 (10 Formosat-2 pixels) and covered by a minimum of 80% of either maize or sunflower pixels were considered in this study.

Each year, this processing provided 40 land use classes, from which maize (grain and silage) and sunflower were extracted. The analysis of the mapped HU showed that:

(i) Sunflower and maize crops covered approximately 21% of the study area.

(ii) Maize was primarily cultivated in the centre of the Formosat-2 images, near the Garonne River. It covered approximately 7700 ha in 2006, 6500 ha in 2007, 7400 ha in 2008 and 6600 ha in 2009. The maize crops were segmented into HU of 2 ha on average. Approximately 95% of these HU were identified as grain maize, the remaining 5% being silage maize.

(ii) Sunflower was cultivated throughout the study area and was dominant over the hill landscapes at the eastern and western part of the study area. Sunflower crops covered approximately 6300 ha in 2006, 5100 ha in 2007, 7200 ha in 2008 and 7200 ha in 2009. Sunflower was segmented into smaller HU than maize of approximately 0.7 ha on average. This was expected as sunflower crops were not irrigated and were often cultivated on hills. Thus, these crops exhibited a higher intra-field variability due to the variation in soil properties and water availability.

2.6. Time series of Green Area Index (GAI)

Many studies have demonstrated the link between spectral vegetation indices (e.g., NDVI, SAVI and EVI) derived from remote sensing observations and the green leaf area index (e.g., Myneni 1994, Weiss et al. 2002, Colombo et al. 2003, Walthall 2004, Duchemin et al. 2006). In our study, the green area index ($GAI_{eff,F2}$) was estimated from the Formosat-2 images using the NDVI and the following exponential relationship (Eq. 1):

$$GAI_{\mathrm{eff,F2}} = k_1 \times e^{k_2 \times NDVI} - k_3 \qquad (1)$$

The coefficients of Eq. 1 were estimated using the minimisation of the root mean square error (RMSE) between $GAI_{eff,CAN\text{-}EYE}$ estimated from the DHPs from the ESUs and $GAI_{eff,F2}$ estimated from Eq. 1. The $GAI_{eff,CAN\text{-}EYE}$ measurements taken more than 4 days after or before the Formosat-2 acquisitions were eliminated from the data set. The NDVI-$GAI_{eff,CAN\text{-}EYE}$ scatterplot is presented in Fig. 4. A single relationship (the black line in Fig. 4) was used for both crops (coefficients k_1=0.35, k_2=2.86, k_3=0.24 in Eq. 1). The RMSE between $GAI_{eff,CAN-EYE}$ and $GAI_{eff,F2}$ was equal to 0.38 $m^2.m^{-2}$ and the relative RMSE (RRMSE) was equal to 20%. The formulation of the equation differed from more commonly used logarithmic formulation. Nevertheless, the current formulation fitted correctly with the in situ measurements of effective GAI. With the current set of coefficients, the GAI estimate could not exceed 5.9 $m^2.m^{-2}$, which was sufficient as it corresponded to effective GAI.

This relationship was then applied to all Formosat-2 pixels. This processing resulted in a time series of effective Formosat-2 GAI (called hereinafter GAI_{F2}), which were spatially averaged over the HU labelled as maize (silage or grain) and sunflower. During the calculation, all of the data with cloudy or shadowed pixels were excluded.

2.7. Calibration of the SAFY model

The simple algorithm for yield estimates (SAFY) is a daily time step model that simulates time series of leaf area index and dry aboveground biomass from the air temperature and the global incoming radiation. An overview of the model is provided in the Appendix 1; a full description is available in Duchemin et al. (2008a).

The model was parameterised for each HU labelled as maize (silage or grain) or sunflower using meteorological data derived from SAFRAN. The thirteen parameters of the SAFY model are listed in Table 2. Initial values were put based on a literature review and field measurements for eight parameter and the six major parameters, identified by Duchemin et al. (2008a), were calibrated using only time series of green area index derived from Formosat-2 images (GAI_{F2}).

2.7.1. Calibration of parameters through literature review and field measurements

The common value of 0.48 was used for the climatic efficiency (Varlet-Grancher et al. 1982). As in Duchemin et al. (2008a), the initial dry aboveground biomass was set arbitrarily to correspond with a GAI of 0.1 $m^2.m^{-2}$.

The three critical temperature values (T_{min}, T_{max}, T_{opt}, Eq. 3 in the Appendix 1) and the degree of the polynomial function (β) that defines the stress temperature function for each crop were obtained from Drouet and Pages (2003) and from the STICS website (http://www.avignon.inra.fr/agroclim_stics/).

The light-extinction coefficient (k_{ext}) was computed by inverting Beer's law (Eq. 5 in the Appendix 1) using the fraction of absorbed photosynthetically active radiation ($FAPAR_{daily,CAN\text{-}EYE}$) and the effective green area index ($GAI_{eff,CAN\text{-}EYE}$) from CAN-EYE. The specific leaf area (SLA) were estimated from measurements of leaf biomass and leaf area done at Lamothe in 2006 (maize) and at Auradé in 2007 (sunflower). Only measurements before the maximum GAI were considerate.

2.7.2. Calibration of parameters based on remote sensing data

The remaining parameters (Pl_a, Pl_b, Stt, Rs, D_0 and ELUE) were all retrieved using only GAI_{F2} time series derived from Formosat-2 images. To limit compensation during the optimisation procedure (see Duchemin et al. 2008a), we classified the parameters in two groups: crop-specific and field-specific parameters. Two corresponding phases were used for the calibration. The methodology of the calibration is described in the Fig. 5. The four crop specific parameters (Pl_a, Pl_b, Stt, Rs), which constrain the shape of the GAI_{F2} time course, were calibrated, on phase 1, separately for sunflower, grain maize and silage maize. The two field specific parameters (D_0 and ELUE) were calibrated, on phase 2, for each HU.

Prior to the calibration procedure, a delimitation of the growing period was needed (Fig. 6). The day of maximum GAI_{F2} (DoY 218 in Fig. 6) was first identified. The algorithm then seeks backward from this day to determine the starting day of the growing period (DoY 156 in Fig. 6), which was defined as the day that exhibited a GAI_{F2} value less than a user-defined threshold. This threshold was set as the minimum GAI_{F2} value, encountered in the backward seek, plus 0.1. The end of the growing season (DoY 288 in Fig. 6) was identified in a similar way, seeking forward before the day of maximum GAI_{F2}. The GAI_{F2} values that did not belong to the identified growing period were excluded (plus symbols in Fig. 6).

The calibration of SAFY was then performed by minimising the Root Mean Square Error (RMSE) between the "cleaned" GAI_{F2} time series and the GAI simulated by SAFY. The minimisation procedure was based on an adapted version of the simplex method (Lagarias et al. 1998), which was run 50 times with a random determination of initial values to avoid stops in local minima.

Intervals of acceptable values were defined for each parameter (Table 2). These intervals were constant for all of the parameters except the date of emergence, for which the interval was established independently for each HU to plus or minus 20 days around the start of the growing period.

The crop-specific parameters were estimated, on phase 1 of the calibration (see Fig. 5), using the GAI_{F2} time series of the 6032 HU deduced from the 2006 Formosat-2 data set. This data set was preferred as it contained a high number of images regularly distributed during the whole growing season. Depending on the HU, 18 to 28 cloud-free images were available from May to September. HU with maximum GAI_{F2} less than 1 $m^2.m^{-2}$ or that lead to RMSE superior to 0.38 $m^2.m^{-2}$ were not kept in our analysis as they were considered to be incorrectly classified. However, an important set (95 %) of crop-specific parameters (Pl_a, Pl_b, Stt, Rs) was available for each crop: 1980 for grain maize, 97 for silage maize and 3644 for sunflower. A median value was then computed for each crop and used on phase 2 of the calibration (see Fig. 5) to constrain the estimation the field-specific parameters (D_0 and ELUE). These latter parameters were estimated per year and per spatial pattern: HU for Formosat-2 footprint estimates, and transect, ESU and field for local estimates. The minimisation procedure of phase 2 was based on a regular simplex method because there is no compensation between these two parameters (Duchemin et al. 2008a).

3. Results and discussion

In this section, results of the calibration and the validation are discussed. The two parameters, estimated from in situ measurements are first discussed. The parameters, estimated from the GAI_{F2} are then described: crop-specific (Pl_a, Pl_b, Stt and Rs) and field-specific (ELUE and D_0). Finally, the validations at local and regional scales are described in the two last sections.

3.1. Light-extinction coefficient and Specific Leaf Area

Fig. 7 displays the relationship between the fraction of absorbed photosynthetically active radiation ($FAPAR_{daily,CAN\text{-}EYE}$) and the effective green area index ($GAI_{eff,CAN\text{-}EYE}$). A single relationship was used for both crops. The best agreement was obtained using a light-extinction coefficient (K_{ext}) of 0.63 (see Eq. 5 in the Appendix 1). The RMSE between FAPAR derived from this relationship and $FAPAR_{daily,CAN\text{-}EYE}$ was 0.033.

The relationship between the leaf area and leaf mass is displayed in Fig. 8. These two variables were linearly related. SLA values corresponding to the slopes of the relationships (Fig. 8) were used in the SAFY simulations: 0.012 $m^2.g^{-1}$ for sunflower and 0.024 $m^2.g^{-1}$ for maize.

3.2. Crop-specific parameters

Fig. 9 shows the box and whiskers plots of the distributions of the crop specific parameters (Pl_a, Pl_b, Stt and Rs) for maize (grain: M and silage: SM) and sunflower (SF) based on phase 1 of the calibration applied on the 5721 HU of the 2006 Formosat-2 data set. Their median values are reported in Table 2 and the distributions appeared very scattered. As previously suggested by

Duchemin et al. (2008a), part of this scattering can be attributed to parameter compensations occurring during the minimisation procedure. The parameters appeared more scattered for sunflower than for maize likely because sunflower crops, which are not irrigated, are much more sensitive to the spatial distribution of rainfall and to soil water content than is maize. They thus experienced larger variations in the GAI_{F2} time series.

"Typical" maize (grain and silage) and sunflower GAI_{F2} time series computed from three HU of the 2006 Formosat-2 data set are plotted on Fig. 10. The analysis of Fig. 9, Fig. 10 and Table 2 revealed that significant information could be derived from the distributions of the crop specific parameters:

(i) The dry aboveground biomass allocated to the leaf at plant emergence ($1-Pl_a$) was 65% for grain maize, 66% for silage maize and 84% for sunflower (Fig. 9). These values were consistent with the ratios of the leaf mass to the dry aboveground biomass derived from *in situ* measurements at the beginning of the agricultural season, which were 75% for maize (Lamothe in 2006) and 83% for sunflower (Auradé in 2007).

(ii) No significant difference was observed between the grain and silage parameters, except the rate of senescence (Rs in Table 2), which was approximately 15 times higher for silage maize. This very high rate of senescence for silage maize corresponded with the sudden drop of GAI_{F2} due to harvesting as illustrated in Fig. 10. Silage maize is used to feed animals and thus it is harvested earlier than grain maize, when grain humidity reaches 80%.

(iii) Senescence began earlier for sunflower than for maize. The threshold of cumulated temperature to initiate senescence was estimated to be 70% lower for sunflower than for maize (Stt in Table 2). This difference is well illustrated in the GAI_{F2} time series (Fig. 10) and was previously shown by Andrade (1995).

3.3. Field specific parameters

The cumulated distribution of the effective light-use efficiency (ELUE) and the emergence dates (D_0) estimated for the sunflower and maize crops of the Formosat-2 footprint are presented in Fig. 11 (a to d). Numbers of HU used to compute the cumulated distribution are shown in the Fig. 11 (a and b). The cumulated distributions of the maximum GAI (GAI_{max}), the rainfall and the temperature stress factor are also plotted (Fig. 11 e to j). The rainfall was cumulated from 30 days before emergence to senescence. The temperature stress factor corresponds to the average of the F_T function (Eq. 3 in the Appendix 1) from emergence to senescence.

The median value of the ELUE averaged over the four years was 3.3 $g.MJ^{-1}$ for maize (Fig. 11a) and 2.0 $g.MJ^{-1}$ for sunflower (Fig. 11b). The SAFY model thus appeared adequate to reproduce the basic difference in photosynthetic rate between maize (C4 plant) and sunflower (C3 plant). The ELUE values for sunflower increased from 2006 to 2008 in relation with the increasing values of cumulated rainfall (Fig. 11h). This is consistent as this parameter is expected to include water stress effect. A similar positive correlation was observed between the median values of cumulated rainfall and GAI_{max} (Fig. 11f). In contrast, the inter-annual variation in maize ELUE was not related to the rainfall. This is consistent as maize is irrigated to avoid water stress. The analysis of the distribution of GAI_{max} (Fig. 11e) permitted the explanation of the inter-annual maize ELUE variations. In 2006 and 2009, the GAI_{max} values were similar despite differences in temperature stress factors, which were highest in 2009 (Fig. 11i). Thus, the calibration procedure induced highest ELUE values in 2009 (Fig. 11a) to compensate for the negative effect of low temperatures on GAI. The same trend was observed in 2007 and 2008; the highest values of temperature stress factor and ELUE were found in 2007. These results revealed that the GAI_{max} is a good indicator of water or temperature stresses and that the model and the calibration procedure proposed here were able to reproduce such effects.

The emergence dates (D_0) were also significantly different between maize (Fig. 11c) and sunflower (Fig. 11d). For maize, the median value was stable over the years and was approximately 164 (June, 13). The plant emergence always occurred within a limited time period; each year, 90% of all of the D_0 values were within +/- 15 days of the annual median value. For sunflower, D_0 was more variable and 90% of the D_0 values were within +/- 45 days of the annual median value. This was consistent with difference in irrigation between the crops; sunflower is not irrigated and thus is more sensitive to the spatial variability of rainfall events and soil properties, which may induce strong differences between fields.

3.4. Evaluation of the simulated GAI and DAM time series at local scale

A quantitative evaluation of the model was performed by comparing the dry aboveground biomass (DAM) simulated by SAFY with those estimated from field measurements. The spatial pattern used for the validation corresponded to the footprint of in situ data: transect, ESU and field. The model was calibrated using the GAI_{F2} time series averaged over the pixels that encompassed transects (sunflower at Auradé in 2007 and maize at Lamothe in 2006 and 2008), over a 3x3 pixel window centred on the ESUs (2008 and 2009) or over the pixels that encompassed fields where grain yields were collected. The GAI_{F2} and DAM time series from 2006 to 2008 resulting from this processing are displayed in Fig. 12.

The analysis of the simulated GAI time series confirmed that the SAFY model was able, after calibration, to reproduce the large range of the observed GAI_{F2} shapes. The maximum GAI_{F2} values of maize were quite low (< 3.5 $m^2.m^{-2}$), which is expected as effective values are proven to underestimate destructive values. This underestimation could reach 30% for the maize and 16% for the sunflower as shown by Demarez et al. (2008). The continuous GAI increase during leaf growth appeared to be accurately reproduced for all of the crops. The difference observed in the time duration of maximal GAI between the sunflower and the maize is also well reproduced. Finally, the GAI decrease during the senescence period was correctly simulated for all crops except for the sunflower crop in 2008 (case 6, Fig. 12); the observed sudden decrease was not simulated by the SAFY model. Hemispherical photographs (Fig. 13) taken in 2008 on July 17 and 24 (referred to as A and B in Fig. 12) revealed that the NDVI and GAI decrease corresponded with flowering.

The temporal dynamics of DAM were correctly reproduced in most of cases. Most of the simulated values ranged within the averages plus or minus the standard deviation of the field measurements. However, some discrepancies were noted:

(i) In 2008, the maximum DAM produced by the grain maize (case 3, Fig. 12) was underestimated by approximately 29% in relative terms. The deviation may be explained by the lack of consideration of an increase of the light use efficiency (LUE) allocated to shoot biomass at the end of the cycle, due to the cessation of root growth. At the opposite, the simulated LUE ($F_T \times$ ELUE) decreases from September as the air temperature decreases.

(ii) In contrast with maize, the maximum DAM produced by sunflower (cases 4 and 6 in Fig. 12) were overestimated. The maximum dry aboveground biomass was unfortunately not measured for case 5. Recent work by Lecoeur et al. (2011) performed with similar sunflower varieties showed that ELUE decreases from the flowering phase, probably in favour of lipids production. The slight decrease in DAM observed before senescence in the measured biomass was due to measurement errors.

The global comparison between simulated and measured DAM from 2006 to 2009 is presented on Fig. 14 and Table 3. There is a good agreement between simulations and field measurements, with a high correlation (r^2 = 0.92, p-value<0.001), almost no bias (- 0.02 $kg.m^{-2}$) and an error (RMSE) of 0.21 $kg.m^{-2}$. The correlation is higher for silage maize (r^2 = 0.96; RRMSE = 11%) than for grain maize (r^2 = 0.86; RRMSE = 26%) and sunflower (r^2 = 0.78; RRMSE = 39%). The global accuracy of simulations (RRMSE = 28% on Fig. 14) was satisfactory considering that the most sensitive parameters of the model were only calibrated with remote sensing observations. This accuracy was comparable to that of studies using more complex models with a large in situ data set. They found accuracy of 14% and 32% for maize using SWATRER-SUCROS and CERES (Xevi et al. 1996), 16% using STICS (Brisson et al. 2002) and 23% using EPIC (Cabelguenne et al. 1999). An accuracy of 21% was found for sunflower using EPIC (Cabelguenne et al. 1999).

The SAFY model was also run for fields for which farmers provided grain yields. The in situ grain yields were compared with the maximum simulated DAM (Fig. 15). The data for sunflower were highly scattered. This was partially due to the overestimations of the SAFY biomass and partially due to uncertainties in the in situ grain yields. For maize, too few measurements were available to exhibit a trend. Despite these limitations, a mean harvest index (HI) was computed for each crop as the ratio of in situ grain yields to the maximum DAM. This index was 0.48 for grain maize and 0.25 for sunflower. The HI calculated for maize appeared consistent with those from previous experimental or modelling studies; Cabelguenne et. al (1999) reported a value of 0.5. Due to the SAFY biomass overestimation, the HI calculated for sunflower was very low compared with the in situ values given by Casadebaig (2008), which varied between 0.35 and 0.45.

3.5. Evaluation of the simulated DAM and grain yield over the Formosat-2 footprint

The distributions of the maximum aerial dry biomass (DAM_{max}) estimated over the whole Formosat-2 footprint are presented in Fig. 16. For sunflower, the maximum DAM values (Fig. 16b) were reached during the wettest year (2008, Fig. 11h). In 2007, despite the strong rainfall, the DAM_{max} values were not as high as in 2008. In 2007, we noticed that the period of emergence was quite long, up to 200 days (Fig. 11d). This was due to heavy rains during the spring, which limited plant emergence, particularly in clay soils, and thus limited the crop production. For maize, the highest maximum DAM values were reached during the hottest years (Fig. 11i).

The DAM_{max} values averaged over four years were equal to approximately 19.5 $t.ha^{-1}$ for maize and 9.6 $t.ha^{-1}$ for sunflower. The grain yields calculated from these averaged DAM_{max} values using the harvest index previously estimated (0.48 for maize and 0.25 for sunflower) were 10.1 $t.ha^{-1}$ for maize and 2.4 $t.ha^{-1}$ for sunflower and were in agreement with the values given by the French Agricultural Statistics for the whole department of Haute-Garonne, which were 10.2 $t.ha^{-1}$ for maize and 2.3 $t.ha^{-1}$ for sunflower (Fig. 17, Agreste 2011). The accuracy of the sunflower grain yield estimation was due to compensation between the overestimated biomass and the underestimated harvest index. Nevertheless, the inter-annual variations of the estimated sunflower grain yields were highly correlated with the reported statistics ($r = 0.97$, p-value<0.03, Fig. 17). The lowest simulated grain yields were found in 2006 which was the driest year (Fig. 11h) like in the reported statistics; the highest simulated grain yields were found in 2008 which was the wettest year like in the reported statistics.

In contrast with sunflower, the inter-annual variation in the maize grain yields did not match the reported grain yield statistics (r = -0.81, Fig. 17). The lowest simulated grain yields were found in 2008, which was the year with the highest reported grain yields. The highest simulated grain yields were estimated for 2009, which had the lowest reported grain yields. As discussed previously, there was a clear effect of temperature on maize leaf and biomass production. We may notice that the reported statistics are given for the entire department of Haute-Garonne, which covers an area much larger than the Formosat-2 footprint. In contrast with the sunflower crops, which are mainly located in the northern part of the department, the maize crops are distributed throughout the department, which exhibits a strong spatial gradient in air temperatures. The mean air temperatures were cumulated during the growing period using the SAFRAN data. They varied from 2419 °C (in 2007) to 2646 °C (in 2006) in the northern part of the department and from 2001 °C (in 2007) to 2202 °C (in 2006) in the southern part of the department. The differences observed in cumulative temperature between the northern and the southern part of the department could reach 400 °C. The Formosat-2 footprint was located in the northern part of the department with a cumulative air temperature varying from 2353 °C (in 2007) to 2600 °C (in 2006). Thus, the SAFY simulations performed over the maize crops were considered to not be representative of the entire department of Haute-Garonne and thus unfortunately not comparable with the reported statistics.

4. Conclusion

In this study, we evaluated the combined use of high spatial and temporal resolutions remote sensing data and a simple crop model to estimate maize and sunflower crops production. A semi-empirical crop model (SAFY, Duchemin et al. 2008a) was calibrated with high temporal and spatial resolution Formosat-2 data available from 4 years (2006 to 2009). The results revealed that the high frequency of the 2006 Formosat-2 data set (27 cloud free images throughout the year) permitted the estimation of phenological parameters (Pl_a, pl_b, Stt and Rs), which were proven to be crop dependant. Once calibrated, these parameters were used to calibrate effective light-use efficiency (ELUE) and emergence dates (D_0), and to simulate biomass from 2006 to 2009. From 2007 to 2009, fewer images were available, but the method remained robust because it relied on the pre-calibration of the phenological parameters using the 2006 high temporal resolution data set. Analysis of the ELUE values showed that the SAFY model was able to reproduce the basic difference in photosynthetic rate between maize (C4 plant) and sunflower (C3 plant). The simulation of D_0 revealed higher variability of non-irrigated sunflower than irrigated maize. The SAFY model was also able to reproduce the temporal variability of GAI_{F2} shape and dry aboveground biomass through the 4 studied years. The errors retrieved from the comparison between destructive sampling and simulated biomass were consistent (RMSE = 0.22 kg.m^{-2}; RRMSE = 29%) in comparison with the values given by authors who used more complex models. However, this approach faced some limitations. First, the use of the 2006 Formosat-2 data set to calibrate phenological parameters (Pl_a, pl_b, Stt and Rs) is a potential source of error. Indeed, the unusual hot at dry meteorological conditions of 2006 impacted the value of calibrated parameters and, thus, all estimations of biomass. Secondly, in the SAFY model, the ELUE is constant over the phenological cycle, which could lead to errors in the dry aboveground biomass estimations. For example, Lecoeur et al. (2011) showed that the ELUE of sunflower decreased during the maturity phase. We consequently suggest a future adaptation of the SAFY model by implementing variation with time for ELUE particularly after flowering. The results also showed that the maximum GAI_{F2} value was a good indicator of the canopy water and temperature stress. Thus the need of a temperature stress function like used into the SAFY model should be questioned through further studies.

Finally, inter-annual variation in grain yields over the entire Formosat-2 data set of images (24 x 24 km²) was estimated using maize and sunflower and compared with grain yield statistics given by the French Agricultural Statistics for the entire department of Haute-Garonne (6300 km²). The SAFY model was able to correctly reproduce the inter-annual variation in the grain yield of sunflower (r^2 = 0.89). In contrast, the inter-annual variation of maize grain yield was not correctly reproduced because of the lack of spatial representativeness of our model simulations.

This study demonstrates the great potential for the use of high spatial and temporal resolution remote sensing data for large-scale crop monitoring. Nevertheless, the high spatial resolution was not fully exploited as simulations were carried out over homogenous unit. Future studies could focus on analysing the intra-field variability by applying such approach at pixel level. Future satellite missions such as Venµs (Dedieu et al. 2006) and Sentinel-2, which will provide high spatial and temporal resolution images with a 4/5 days revisiting period and with a high number of spectral bands (12/13 spectral bands), will offer new perspectives for such applications.

Acknowledgements

This work was made possible through the support of the European Commission (FEDER Interreg IVa program, ref POCTEFA 08/34, Fluxpyr), the French Ministry in Charge of Research ("Réseau Terre et Espace"), the Centre National de la Recherche Scientifique (CNRS), the Institut National des Sciences de l'Univers (INSU), the Centre National d'Etudes Spatiales (CNES) and the Région Midi-Pyrénées Council. We are very grateful to the farmers of Auradé and Lamothe and to Michel Gay from E.I. Purpan for granting and facilitating our access to their fields. We also express gratitude to Eric Martin from CNRM-GAME (Météo France) for providing the SAFRAN meteorological data. We finally would like to thank Marie Weiss and Frédéric Baret from EMMAH (INRA Avignon) for the support on CAN-EYE software. Special thanks to our technical staff: Hervé Gibrin, Nicole Ferroni and Bernard Marciel.

References

Agreste (2011). La statistique Agricole. *Ministère de l'agriculture et de la pêche*. http://www.agreste.agriculture.gouv.fr, last access: May 2011.

Andrade, F.H. (1995). Analysis of growth and yield of maize, sunflower and soybean grown at Balcarce, Argentina. *Field Crops Research*, *41*, 1-12.

Asrar, G., Fuchs, M., Kanemasu, E.T., & Hatfield, J.L. (1984). Estimating absorbed photosynthetic radiation and leaf-area index from spectral reflectance in wheat. *Agronomy Journal, 76*, 300-306.

Baillarin, S., Gigord, P., & O., H. (2008). Atomatic Registration of optical images, a stake for future missions: application to ortho-rectification, time series and mosaic products. *2008 Ieee International Geoscience and Remote Sensing Symposium*, *Vols 1-8*, 928-931.

Baret, F., & Guyot, G. (1991). Potentials and limits of vegetation indexes for lai and apar assessment. *Remote Sensing of Environment*, *35*, 161-173.

Baret, F., Hagolle, O., Geiger, B., Bicheron, P., Miras, B., Huc, M., Berthelot, B., Nino, F., Weiss, M., Samain, O., Roujean, J.L., & Leroy, M. (2007). LAI, fAPAR and fCover CYCLOPES global products derived from VEGETATION - Part 1: Principles of the algorithm. *Remote Sensing of Environment, 110*, 275-286.

Baret, F., de Solan, B., Lopez-Lozano, R., Ma, K., & Weiss, M. (2010). GAI estimates of row crops from downward looking digital photos taken perpendicular to rows at 57.5 degrees zenith angle: Theoretical considerations based on 3D architecture models and application to wheat crops. *Agricultural and Forest Meteorology*, *150*, 1393-1401.

Basso, B., Ritchie, J.T., Pierce, F.J., Braga, R.P., & Jones, J.W. (2001). Spatial validation of crop models for precision agriculture. *Agricultural Systems*, *68*, 97-112.

Bastiaanssen, W.G.M., Molden, D.J., & Makin, I.W. (2000). Remote sensing for irrigated agriculture: examples from research and possible applications. *Agricultural Water Management*, *46*, 137-155.

Boote, K.J., Jones, J.W., & Pickering, N.B. (1996). Potential uses and limitations of crop models. *Agronomy Journal*, *88*, 704-716.

Brisson, N., Ruget, F., Gate, P., Lorgeau, J., Nicoullaud, B., Tayot, X., Plenet, D., Jeuffroy, M.H., Bouthier, A., Ripoche, D., Mary, B., & Justes, E. (2002). STICS: a generic model for simulating crops and their water and nitrogen balances. II. Model validation for wheat and maize. *Agronomie*, *22*, 69-92.

Brisson, N., Gary, C., Justes, E., Roche, R., Mary, B., Ripoche, D., Zimmer, D., Sierra, J., Bertuzzi, P., Burger, P., Bussiere, F., Cabidoche, Y.M., Cellier, P., Debaeke, P., Gaudillere, J.P., Henault, C., Maraux, F., Seguin, B., & Sinoquet, H. (2003). An overview of the crop model STICS. *European Journal of Agronomy*, *18*, 309-332.

Bsaibes, A., Courault, D., Baret, F., Weiss, M., Olioso, A., Jacob, F., Hagolle, O., Marloie, O., Bertrand, N., Desfond, V., & Kzemipour, F. (2009). Albedo and LAI estimates from FORMOSAT-2 data for crop monitoring. *Remote Sensing of Environment*, *113*, 716-729.

Cabelguenne, M., Debaeke, P., & Bouniols, A. (1999). EPICphase, a version of the EPIC model simulating the effects of water and nitrogen stress on biomass and yield, taking account of developmental stages: validation on maize, sunflower, sorghum, soybean and winter wheat. *Agricultural Systems, 60*, 175-196.

Casadebaig, P. (2008). Analyse et modélisation des interactions génotype - environnement - conduite de culture : application au tournesol (Helianthus annuus). In, *Agrosystèmes et développement territorial (AGIR)*. Toulouse.

Ceschia, E., Beziat, P., Dejoux, J.F., Aubinet, M., Bernhofer, C., Bodson, B., Buchmann, N., Carrara, A., Cellier, P., Di Tommasi, P., Elbers, J.A., Eugster, W., Gruenwald, T., Jacobs, C.M.J., Jans, W.W.P., Jones, M., Kutsch, W., Lanigan, G., Magliulo, E., Marloie, O., Moors, E.J., Moureaux, C., Olioso, A., Osborne, B., Sanz, M.J., Saunders, M., Smith, P., Soegaard, H., & Wattenbach, M. (2010). Management effects on net ecosystem carbon and GHG budgets at European crop sites. *Agriculture Ecosystems & Environment, 139*, 363-383.

Chern, J.S., Wu, A.M., & Lin, S.F. (2006). Lesson learned from FORMOSAT-2 mission operations. *Acta Astronautica, 59*, 344-350.

Colombo, R., Bellingeri, D., Fasolini, D., & Marino, C.M. (2003). Retrieval of leaf area index in different vegetation types using high resolution satellite data. *Remote Sensing of Environment, 86*, 120-131.

Courault, D., Bsaibes, A., Kpemlie, E., Hadria, R., Hagolle, O., Marloie, O., Hanocq, J.F., Olioso, A., Bertrand, N., & Desfonds, V. (2008). Assessing the potentialities of FORMOSAT-2 data for water and crop monitoring at small regional scale in South-Eastern France. *Sensors, 8*, 3460-3481.

Dedieu, G., Karnieli, A., Hagolle, O., Jeanjean, H., Cabot, F., Ferrier, P., & al., e. (2006). VENμS: A joint Israel–French Earth Observation scientific mission with High spatial and temporal resolution capabilities. In, *Second Recent Advances in Quantitative Remote Sensing symposium*. Torrent.

Demarez, V., Duthoit, S., Baret, F., Weiss, M., & Dedieu, G. (2008). Estimation of leaf area and clumping indexes of crops with hemispherical photographs. *Agricultural and Forest Meteorology, 148*, 644-655.

Dolman, A.J., Noilhan, J., Durand, P., Sarrat, C., Brut, A., Piguet, B., Butet, A., Jarosz, N., Brunet, Y., Loustau, D., Lamaud, E., Tolk, L., Ronda, R., Miglietta, F., Gioli, B., Magliulo, V., Esposito, M., Gerbig, C., Korner, S., Glademard, R., Ramonet, M., Ciais, P., Neininger, B., Hutjes, R.W.A., Elbers, J.A., Macatangay, R., Schrems, O., Perez-Landa, G., Sanz, M.J., Scholz, Y., Facon, G., Ceschia, E., & Beziat, P. (2006). The CarboEurope regional experiment strategy. *Bulletin of the American Meteorological Society, 87*, 1367-+.

Dong, J.R., Kaufmann, R.K., Myneni, R.B., Tucker, C.J., Kauppi, P.E., Liski, J., Buermann, W., Alexeyev, V., & Hughes, M.K. (2003). Remote sensing estimates of boreal and temperate forest woody biomass: carbon pools, sources, and sinks. *Remote Sensing of Environment, 84*, 393-410

Drouet, J.L., & Pages, L. (2003). GRAAL: a model of GRowth, Architecture and carbon ALlocation during the vegetative phase of the whole maize plant - Model description and parameterisation. *Ecological Modelling, 165*, 147-173.

Duchemin, B., Hadria, R., Erraki, S., Boulet, G., Maisongrande, P., Chehbouni, A., Escadafal, R., Ezzahar, J., Hoedjes, J.C.B., Kharrou, M.H., Khabba, S., Mougenot, B., Olioso, A., Rodriguez, J.C., & Simonneaux, V. (2006). Monitoring wheat phenology and irrigation in Central Morocco: On the use of relationships between evapotranspiration, crops coefficients, leaf area index and remotely-sensed vegetation indices. *Agricultural Water Management, 79*, 1-27.

Duchemin, B., Maisongrande, P., Boulet, G., & Benhadj, I. (2008a). A simple algorithm for yield estimates: Evaluation for semi-arid irrigated winter wheat monitored with green leaf area index. *Environmental Modelling & Software*, *23*, 876-892.

Duchemin, B., Hagolle, O., Mougenot, B., Benhadj, I., Hadria, R., Simonneaux, V., Ezzahar, J., Hoedjes, J., Khabba, S., Kharrou, M.H., Boulet, G., Dedieu, G., Er-Raki, S., Escadafal, R., Olioso, A., & Chehbouni, A.G. (2008b). Agrometerological study of semi-arid areas: an experiment for analysing the potential of time series of FORMOSAT-2 images (Tensift-Marrakech plain). *International Journal of Remote Sensing*, *29*, 5291-5300.

Durand, Y., Brun, E., Mérindol, L., Guyomarc'h, G., Lesaffre, B., & Martin, E. (1993). A meteorological estimation of relevant parameters for snow models. In (pp. 65-71): Annals of Glaciology.

Faivre, R., Leenhardt, D., Voltz, M., Benoît, M., Papy, F., Dedieu, G., & Wallach, D. (2004). Spatialising crop models. *Agronomie*, *24*, 205-217.

Fieuzal, R., Duchemin, B., Jarlan, L., Zribi, M., Baup, F., Merlin, O., Dedieu, G., Garatuza-Payan, J., Watt, C., & Chehbouni, A. (2010). Combined use of optical and radar satellite data for the monitoring of irrigation and soil moisture of wheat crops. (pp. 6207-6242).

Fjortoft, R., Lopes, A., Bruniquel, J., & Marthon, P. (1999). Optimal edge detection and edge localization in complex SAR images with correlated speckle. *Ieee Transactions on Geoscience and Remote Sensing, 37*, 2272-2281.

Flenet, F., Kiniry, J.R., Board, J.E., Westgate, M.E., & Reicosky, D.C. (1996). Row spacing effects on light extinction coefficients of corn, sorghum, soybean, and sunflower. *Agronomy Journal, 88*, 185-190.

Hadria, R., Duchemin, B., Baup, F., Le Toan, T., Bouvet, A., Dedieu, G., & Le Page, M. (2009). Combined use of optical and radar satellite data for the detection of tillage and irrigation operations: Case study in Central Morocco. *Agricultural Water Management, 96*, 1120-1127.

Hadria, R., Duchemin, B., Jarlan, L., Dedieu, G., Baup, F., Khabba, S., Olioso, A., & Le Toan, T. (2010). Potentiality of optical and radar satellite data at high spatio-temporal resolutions for the monitoring of irrigated wheat crops in Morocco. *International Journal of Applied Earth Observation and Geoinformation, 12*, S32-S37.

Hagolle, O., Dedieu, G., Mougenot, B., Debaecker, V., Duchemin, B., & Meygret, A. (2008). Correction of aerosol effects on multi-temporal images acquired with constant viewing angles: Application to Formosat-2 images. *Remote Sensing of Environment, 112*, 1689-1701.

Hagolle, O., Huc, M., Pascual, D.V., & Dedieu, G. (2010). A multi-temporal method for cloud detection, applied to FORMOSAT-2, VENμS, LANDSAT and SENTINEL-2 images. *Remote Sensing of Environment, 114*, 1747-1755.

Hutchinson, J.J., Campbell, C.A., & Desjardins, R.L. (2004). Some perspectives on carbon sequestration in agriculture. In, *International Workshop on Contribution of Agriculture to the State of Climate* (pp. 288-302). Ottawa, CANADA: Elsevier Science Bv.

Idbraim, S. (2009). Méthodes d’extraction de l'information spatiale et de classification en imagerie de télédétection : Applications à la cartographie thématique de la région d’Agadir (Maroc). In, *Sciences de l’Univers, de l’Environnement et de l’Espace* (p. 149). Toulouse: Université Toulouse III - Paul Sabatier.

Jamieson, P.D., Porter, J.R., Goudriaan, J., Ritchie, J.T., van Keulen, H., & Stol, W. (1998). A comparison of the models AFRCWHEAT2, CERES-wheat, Sirius, SUCROS2 and SWHEAT with measurements from wheat grown under drought. *Field Crops Research, 55*, 23-44.

Kutsch, W.L., Aubinet, M., Buchmann, N., Smith, P., Osborne, B., Eugster, W., Wattenbach, M., Schrumpf, M., Schulze, E.D., Tomelleri, E., Ceschia, E., Bernhofer, C., Beziat, P., Carrara, A., Di Tommasi, P., Gruenwald, T., Jones, M., Magliulo, V., Marloie, O., Moureaux, C., Olioso, A., Sanz, M.J., Saunders, M., Sogaard, H., & Ziegler, W. (2010). The net biome production of full crop rotations in Europe. *Agriculture Ecosystems & Environment, 139*, 336-345.

Lagarias, J.C., Reeds, J.A., Wright, M.H., & Wright, P.E. (1998). Convergence properties of the Nelder-Mead simplex method in low dimensions. *Siam Journal on Optimization, 9*, 112-147.

Lecoeur, J., Poire-Lassus, R., Christophe, A., Pallas, B., Casadebaig, P., Debaeke, P., Vear, F., & Guilioni, L. (2011). Quantifying physiological determinants of genetic variation for yield potential in sunflower. SUNFLO: a model-based analysis. *Functional Plant Biology, 38*, 246-259.

Lindquist, J.L., Arkebauer, T.J., Walters, D.T., Cassman, K.G., & Dobermann, A. (2005). Maize radiation use efficiency under optimal growth conditions. *Agronomy Journal, 97*, 72-78.

Liu, J.G., Pattey, E., Miller, J.R., McNairn, H., Smith, A., & Hu, B.X. (2010). Estimating crop stresses, aboveground dry biomass and yield of corn using multi-temporal optical data combined with a radiation use efficiency model. *Remote Sensing of Environment, 114*, 1167-1177.

Lobell, D.B., Asner, G.P., Ortiz-Monasterio, J.I., & Benning, T.L. (2003). Remote sensing of regional crop production in the Yaqui Valley, Mexico: estimates and uncertainties. *Agriculture Ecosystems & Environment, 94*, 205-220.

Loseen, D., Mougin, E., Rambal, S., Gaston, A., & Hiernaux, P. (1995). A regional sahelian grassland model to be coupled with multispectral satellite data .2. toward the control of its simulations by remotely-sensed indexes. *Remote Sensing of Environment, 52*, 194-206.

Maas, S.J. (1993). Parameterized model of gramineous crop growth .1. leaf-area and dry mass simulation. *Agronomy Journal, 85*, 348-353.

Monteith, J.L. (1977). Climate and efficiency of crop production in britain. *Philosophical Transactions of the Royal Society of London Series B-Biological Sciences, 281*, 277-294.

Moulin, S., Bondeau, A., & Delecolle, R. (1998). Combining agricultural crop models and satellite observations: from field to regional scales. *International Journal of Remote Sensing, 19*, 1021-1036.

Myneni, R.B., & Williams, D.L. (1994). On the relationship between FAPAR and NDVI. *Remote Sensing of Environment, 49*, 200-211.

Pinter, P.J., Hatfield, J.L., Schepers, J.S., Barnes, E.M., Moran, M.S., Daughtry, C.S.T., & Upchurch, D.R. (2003). Remote sensing for crop management. *Photogrammetric Engineering and Remote Sensing*, *69*, 647-664.

Prince, S.D. (1991). A model of regional primary production for use with coarse resolution satellite data. *International Journal of Remote Sensing*, *12*, 1313-1330.

Quintana-Segui, P., Le Moigne P., Durand Y., Martin E., Habets F., Baillon M., Canellas C., Franchisteguy L. & Morel S. (2008). Analysis of near-surface atmospheric variables : Validation of the safran analysis over France, *Journal of Applied Meteorology and Climatology*, 47 (1), 92–107.

Scotford, I.M., & Miller, P.C.H. (2005). Applications of spectral reflectance techniques in Northern European cereal production: A review. *Biosystems Engineering*, *90*, 235-250.

Tucker, C.J., Vanpraet, C., Boerwinkel, E., & Gaston, A. (1983). Satellite remote-sensing of total dry-matter production in the senegalese sahel. *Remote Sensing of Environment*, *13*, 461-474.

Tucker, C.J., & Sellers, P.J. (1986). Satellite remote-sensing of primary production. *International Journal of Remote Sensing*, *7*, 1395-1416.

Varlet-Grancher, C., Bonhomme, R., Chartier, M., & Artis, P. (1982). Efficience de la conversion de l'énergie solaire par un couvert végétal. In (pp. 3-26): Acta Oecologia/Oecologia Plantarum

Walthall, C., Dulaney, W., Anderson, M., Norman, J., Fang, H.L., & Liang, S.L. (2004). A comparison of empirical and neural network approaches for estimating corn and soybean leaf area index from Landsat ETM+ imagery. *Remote Sensing of Environment*, *92*, 465-474.

Weiss, M., Baret, F., Leroy, M., Hautecoeur, O., Bacour, C., Prevot, L., & Bruguier, N. (2002). Validation of neural net techniques to estimate canopy biophysical variables from remote sensing data. *Agronomie, 22*, 547-553.

Wessels, K.J., Prince, S.D., Zambatis, N., Macfadyen, S., Frost, P.E., & Van Zyl, D. (2006). Relationship between herbaceous biomass and 1-km(2) Advanced Very High Resolution Radiometer (AVHRR) NDVI in Kruger National Park, South Africa. *International Journal of Remote Sensing, 27*, 951-973.

Wit de, A.J.W., Boogaard, H.L., & van Diepen, C.A. (2005). Spatial resolution of precipitation and radiation: The effect on regional crop yield forecasts. *Agricultural and Forest Meteorology, 135*, 156-168.

Wylie, B.K., Harrington, J.A., Prince, S.D., & Denda, I. (1991). Satellite and ground-based pasture production assessment in Niger - 1986-1988. *International Journal of Remote Sensing, 12*, 1281-1300.

Xevi, E., Gilley, J., & Feyen, J. (1996). Comparative study of two crop yield simulation models. *Agricultural Water Management, 30*, 155-173.

Figures

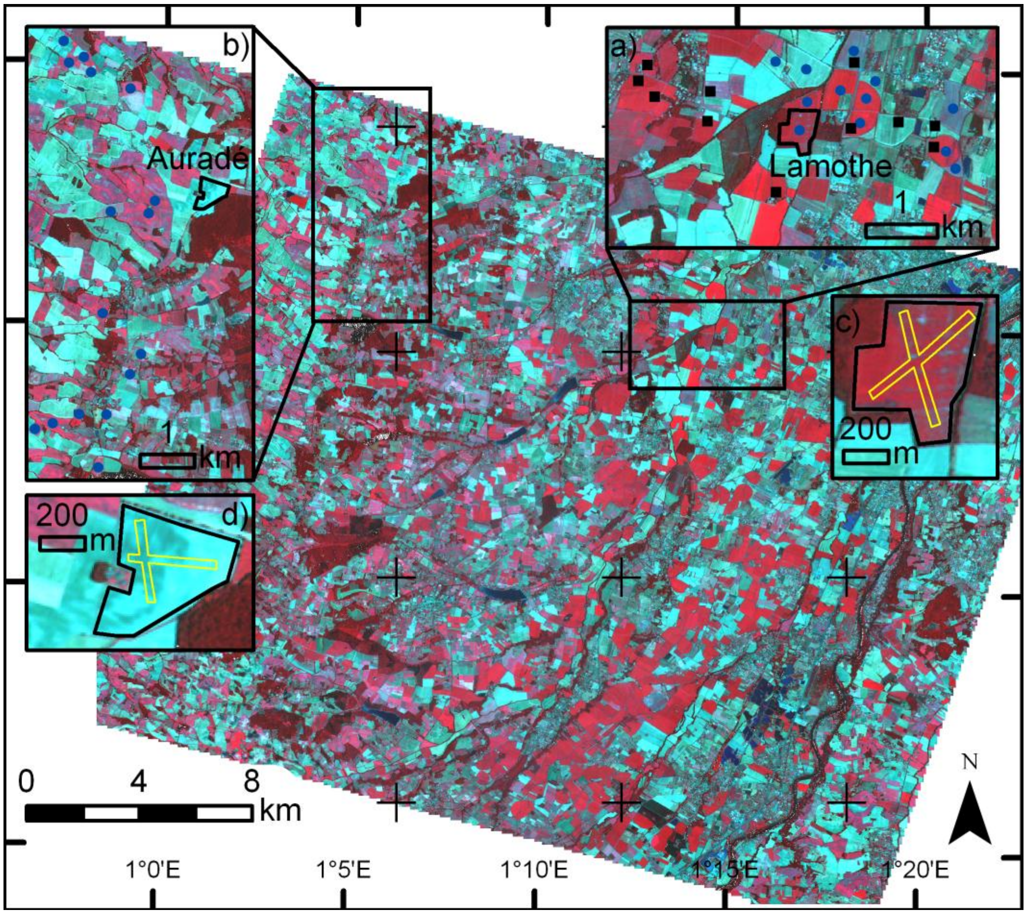

Figure 1: The study area as observed in a Formosat-2 image in July 2008. The areas where field data were collected are shown in a) and b) frames; the black symbols indicate the locations of the elementary sampling units (11 ESUs near Lamothe), and the blue disks indicate the fields for which the farmers provided grain yield data (12 fields near Lamothe, 16 fields near Auradé). The so-called Lamothe (frame c) and Auradé (frame d) fields (delimited with black lines) are experimental fields that belong to the CarboEurope-IP experiment; biomass measurements were performed along transects (in yellow). Black crosses indicate the SAFRAN meteorological grid.

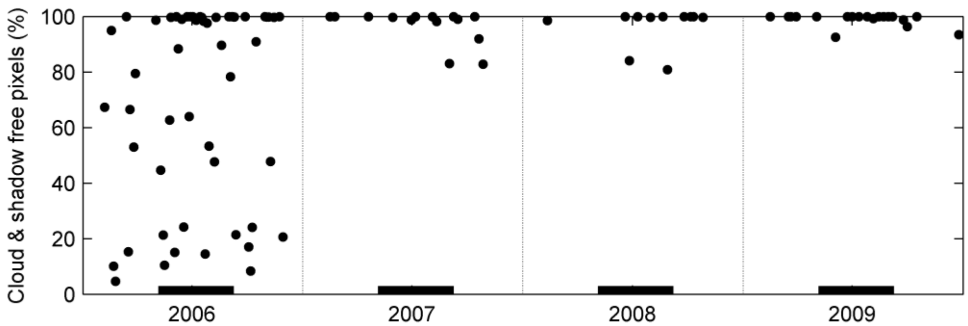

Figure 2: Dates of acquisition of the Formosat-2 images with the corresponding percentage of cloud-free and shadow-free pixels. Thick black lines represent the standard summer crop-growing period (day of year 125 to 250).

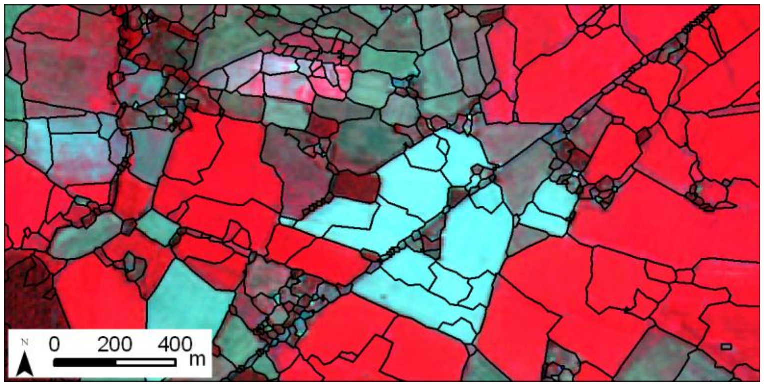

Figure 3: Map of delimitation of Homogenous Unit (black lines). The background corresponds to a Formosat-2 image in July 2008, displayed using a false colour composite.

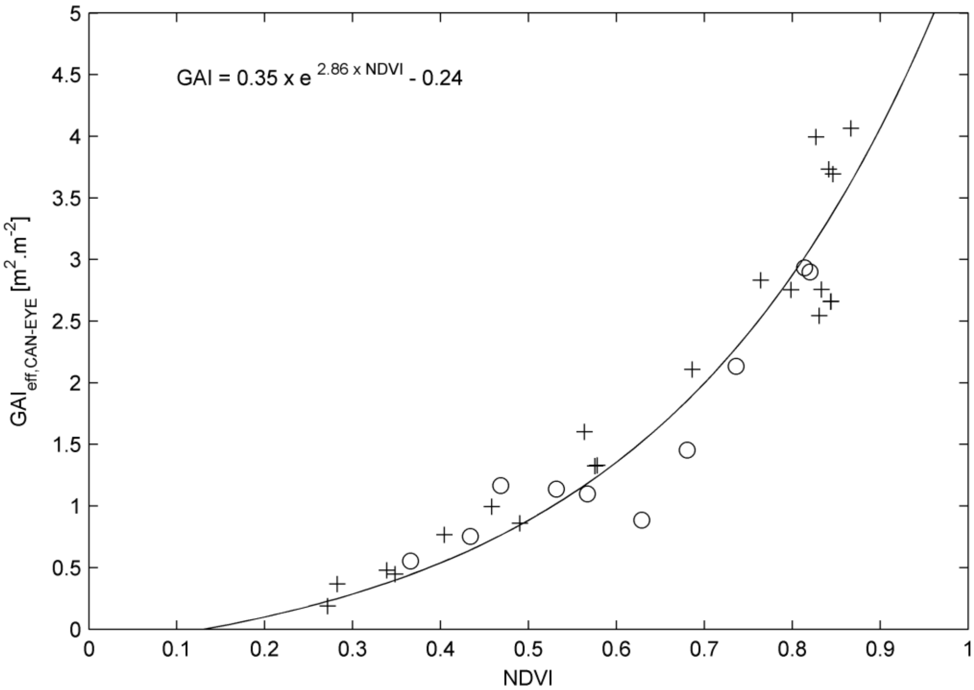

Figure 4: Exponential law (black line) between the effective green area index ($GAI_{eff,CAN-EYE}$) and Formosat-2 NDVI. $GAI_{eff,CAN-EYE}$ were collected per ESU and NDVI were averaged on a 3×3 pixels windows centred on the ESU. Pluses and circles indicate maize and sunflower crops, respectively.

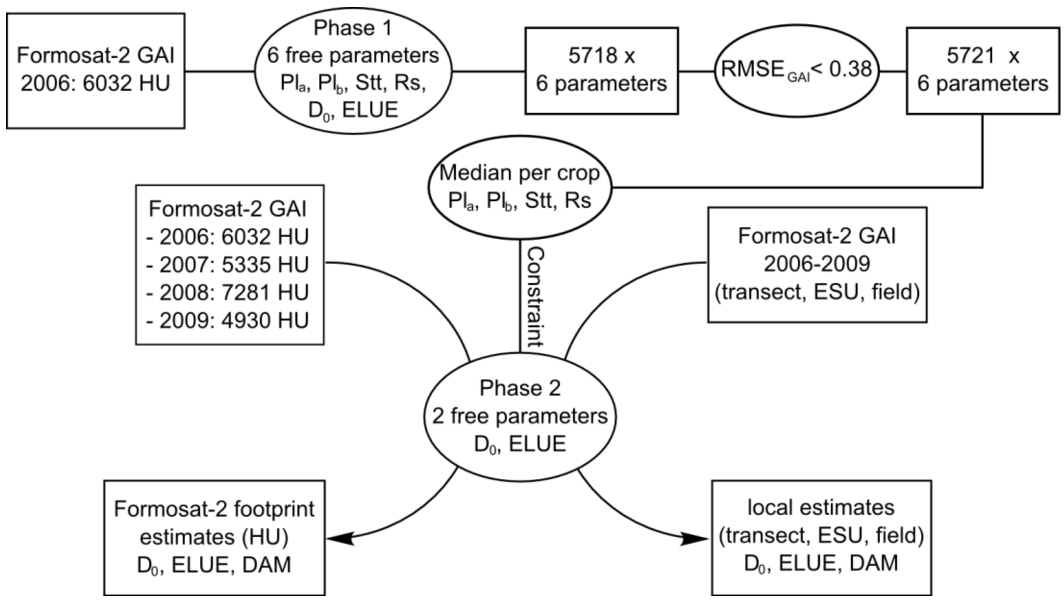

Figure 5: Description of the two phases of the calibration. Phase 1 and 2 describes the calibration of the crop-specific parameters and the field-specific parameters, respectively.

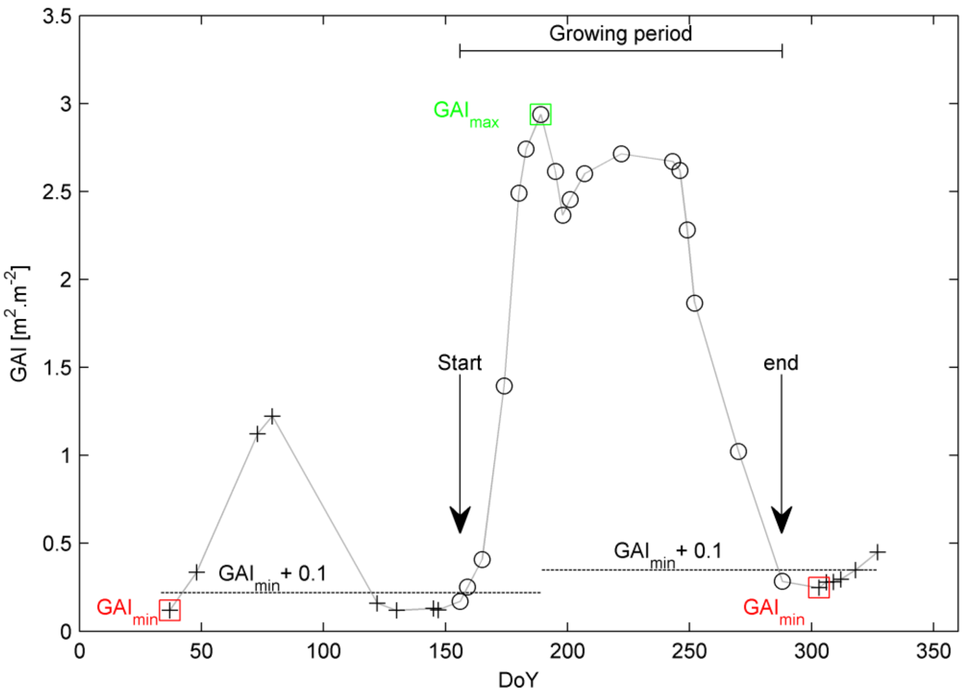

Figure 6: Example of the delimitation of the growing season on a Formosat-2 GAI time series for maize. The dashed line indicates the normal law fitted on the GAI time series. The maximum GAI is framed in green and the two minimum GAI (from each side) are framed in red. The horizontal dashed lines indicate the bare soil thresholds used to detect the start and the end of the growing period. Circles and crosses indicate, respectively, selected and non-selected data acquired within the growing period.

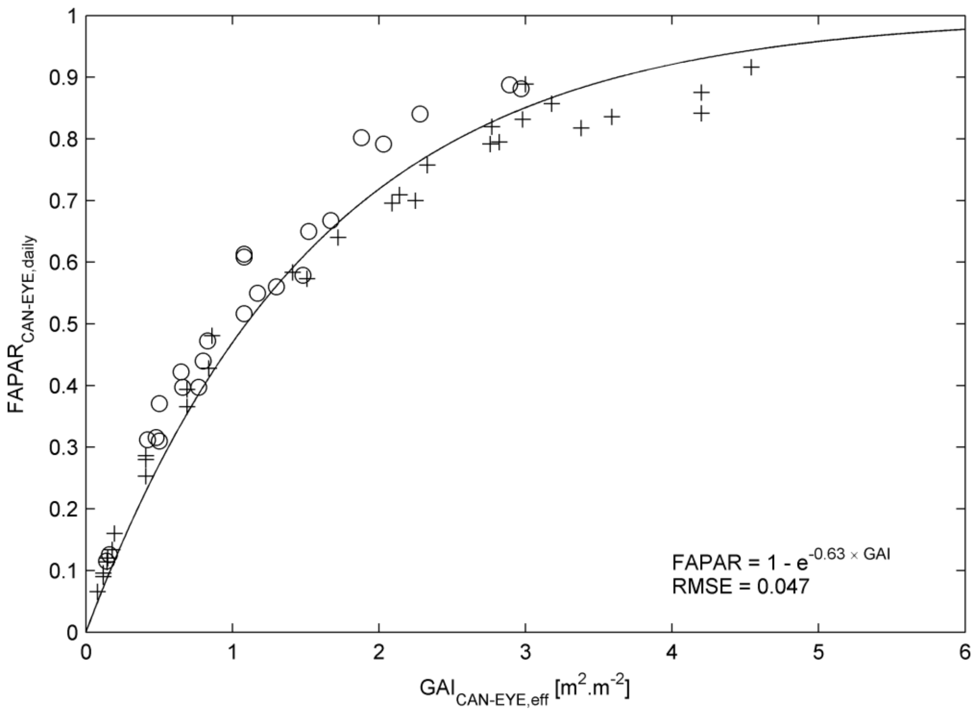

Figure 7: Relationship between the daily fraction of absorbed photosynthetically active radiation (FAPAR$_{daily,CAN-EYE}$) and effective green area index (GAI$_{eff,CAN-EYE}$) derived from the hemispherical photographs. Pluses and circles indicate maize and sunflower crops, respectively.

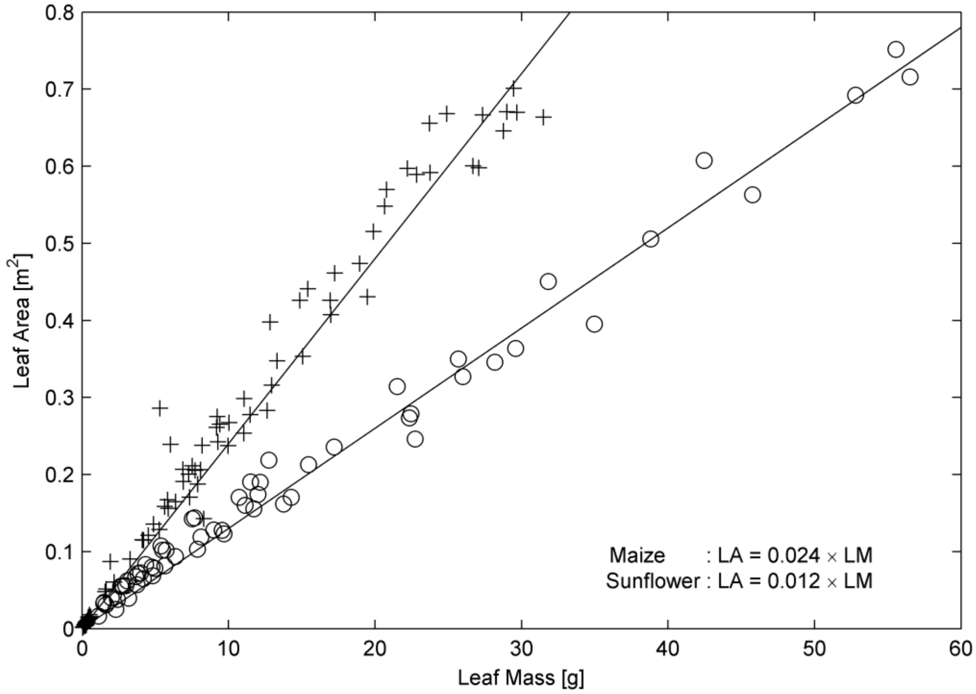

Figure 8: Relationship between leaf area (LA) and leaf mass (LM) estimated from destructive measurements. Pluses and circles indicate maize and sunflower crops, respectively. The slopes of the solid lines correspond to the SLA ($m^2.g^{-1}$) values.

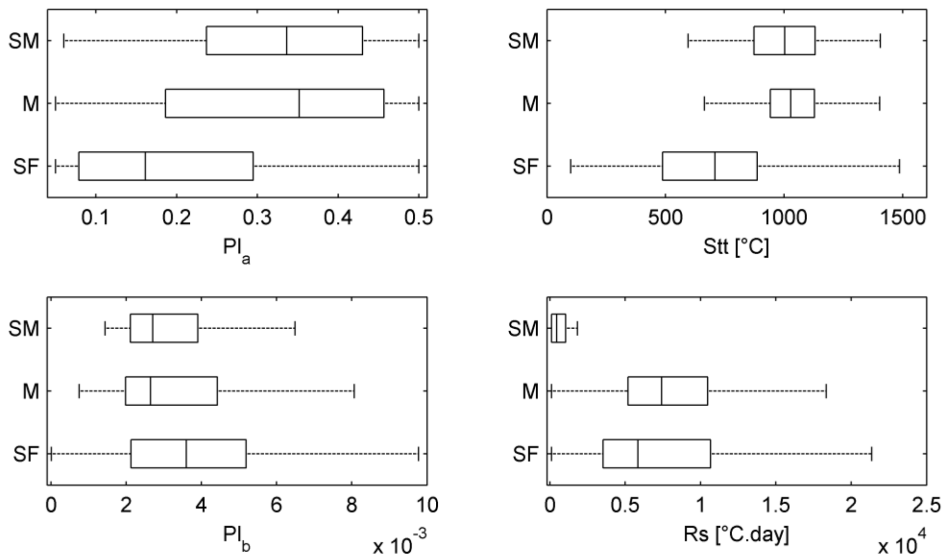

Figure 9: Distributions of crop-specific parameters of maize (grain: M and Silage: SM) and sunflower (SF) based on phase 1 of the calibration applied on the 5721 HU of the 2006 Formosat-2 data set (1980 for grain maize, 97 for silage maize and 3644 for sunflower). Lower and upper quartiles and median values are presented. The whiskers (lines extending from each end of the boxes) show the extent of the rest of the data, excluding outliers (not shown).

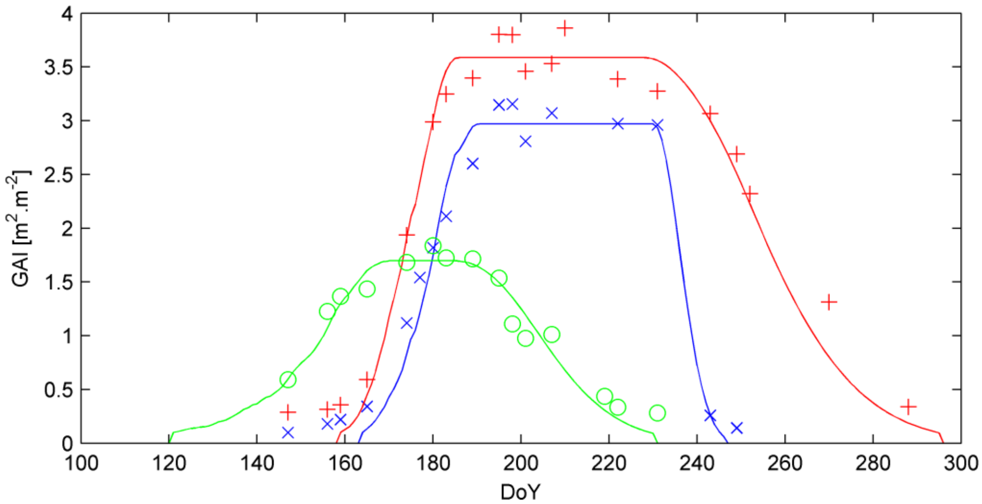

Figure 10: Example of three 2006 Formosat-2 GAI time series. Red pluses, blue crosses and green circles indicate grain maize, silage maize and sunflower, respectively. Full lines show the SAFY simulations.

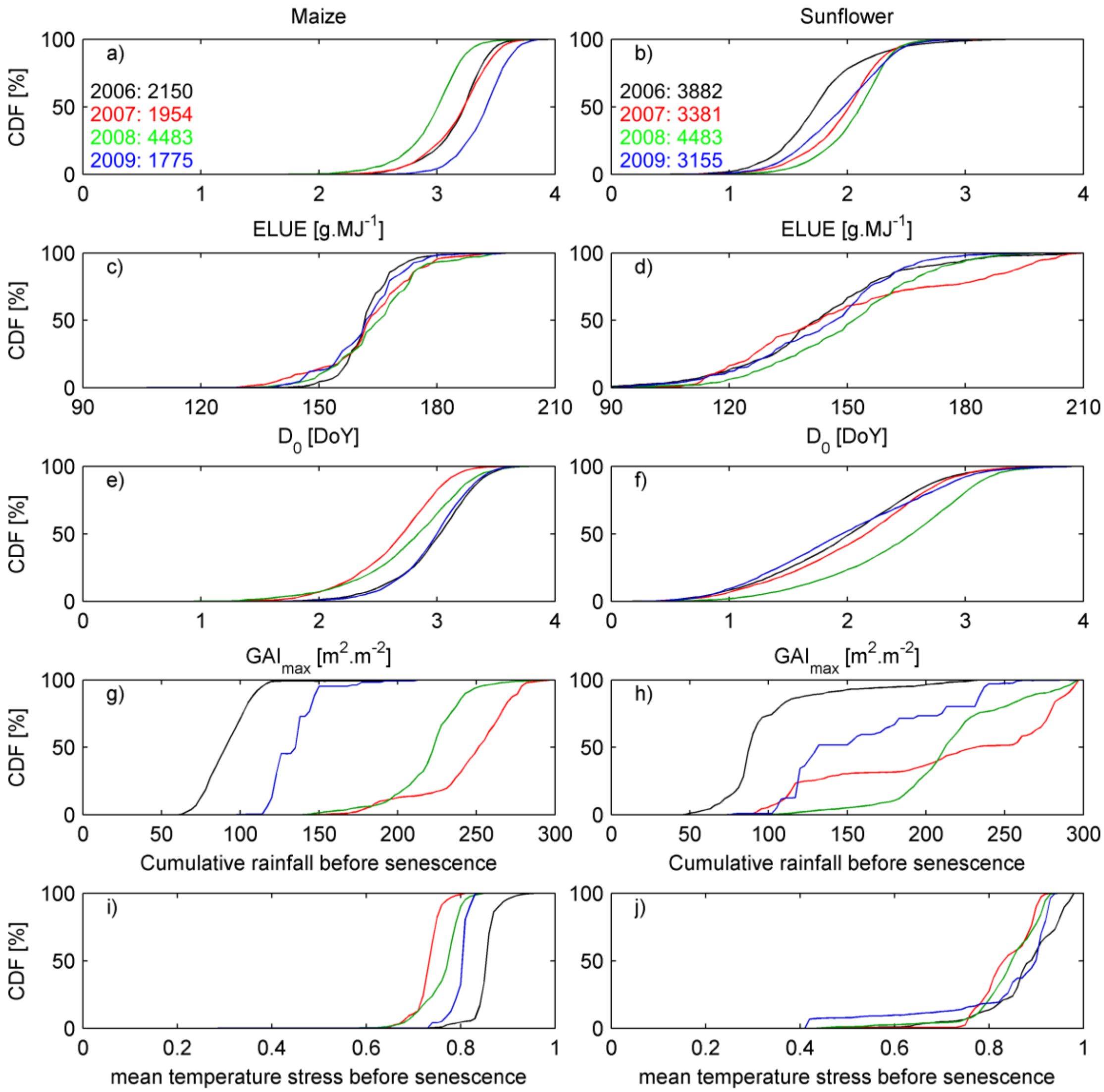

Figure 11: Cumulative distribution function (CDF) of ELUE (a and b), D_0 (c and d) and maximum GAI (GAI_{max}, e and f) simulated for maize (left column) and sunflower (right column) in 2006 (black), 2007 (red), 2008 (green) and 2009 (blue) over the whole Formosat-2 footprint. The rainfall (g and h) was cumulated from 30 days before emergence to the start of the senescence. The mean temperature stress (i and j) was cumulated from emergence to the start of the senescence. The amount of data used is shown in a and b.

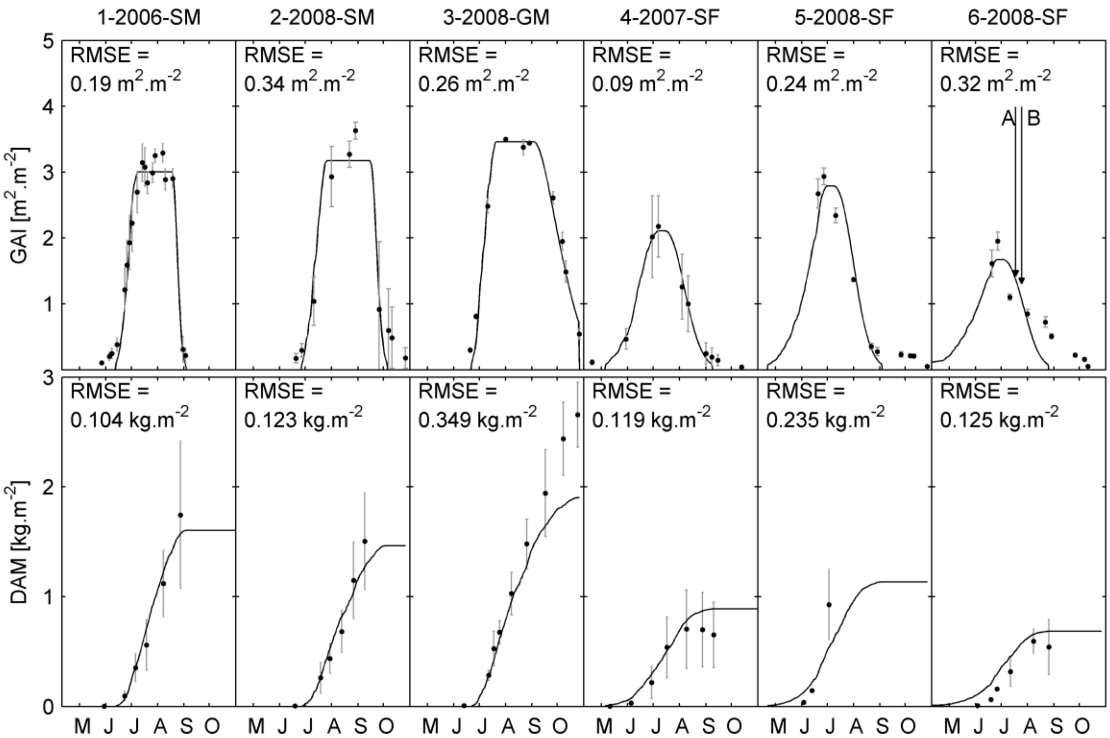

Figure 12: Green area index (GAI) and dry aboveground mass (DAM) simulated (lines) and measured (disks) over 6 experimental fields for the period 2006-2008. M: maize, SM: silage maize and SF: sunflower. Grey error bars on GAI and DAM correspond to the standard deviation computed from the pixels (GAI) and the measurements (DAM) performed either over the transects (cases 1, 2 and 4) or the ESUs (case 3, 5 and 6). A and B, mentioned for case 6, refer to the hemispherical photographs shown in Fig. 13.

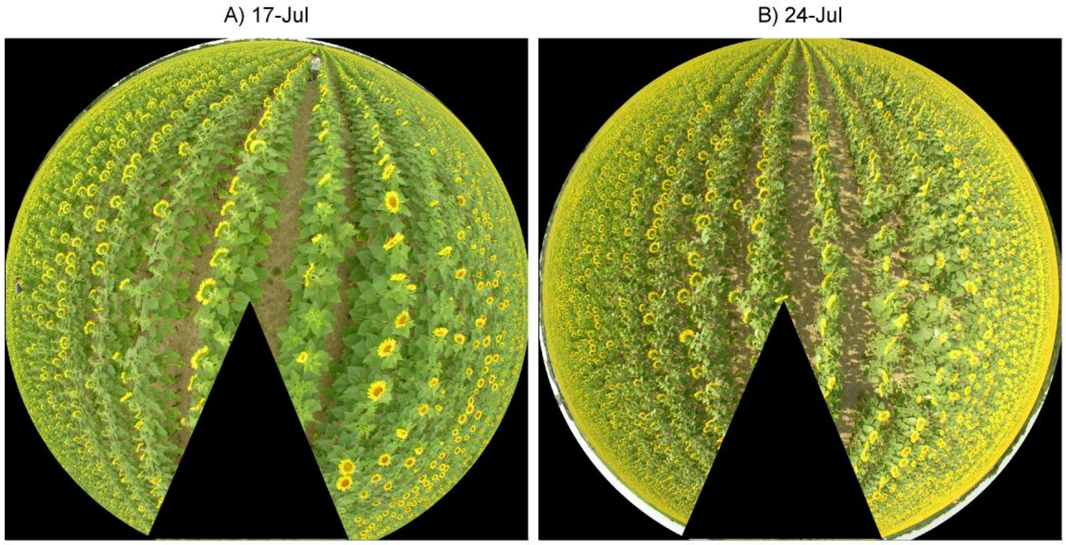

Figure 13: Hemispherical photographs taken in 2008 on July 17 (A) and July 24 (B) over the ESUs corresponding to case 6 of Fig. 12.

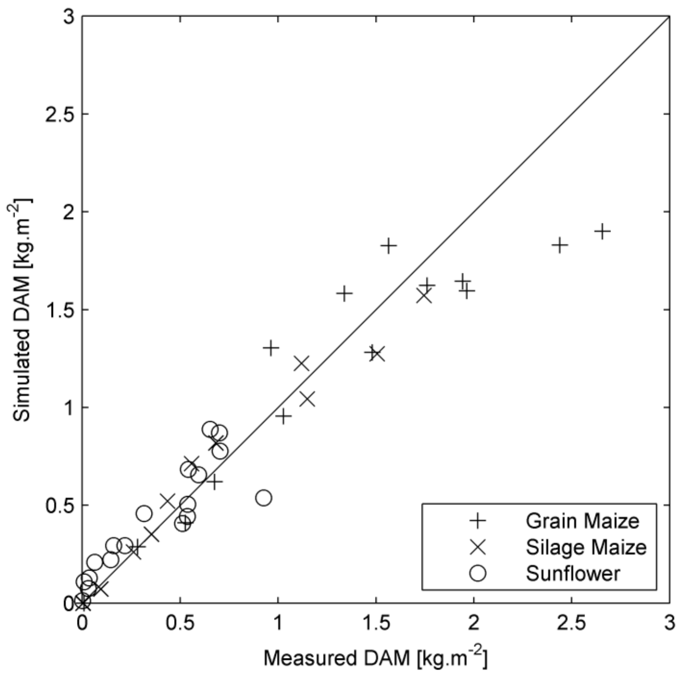

Figure 14: Comparison between the simulated and measured dry aboveground mass (DAM) over all of the experimental fields for the period 2006-2009.

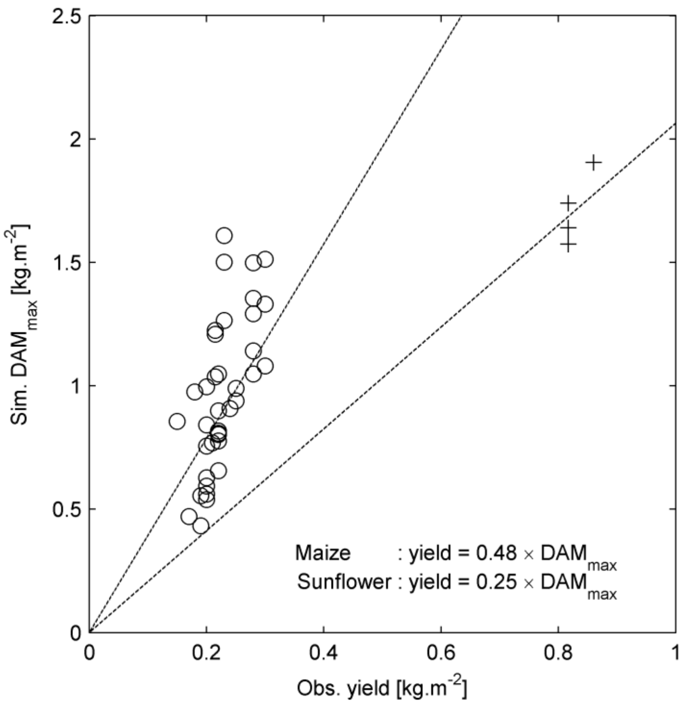

Figure 15: Relationship between simulated maximum dry aboveground mass (DAM_{max}) and grain yields in 2006, 2007 and 2008, provided by farmers for 28 maize (+) and sunflower (o) crops. The slopes of the dashed lines correspond to the mean harvest index.

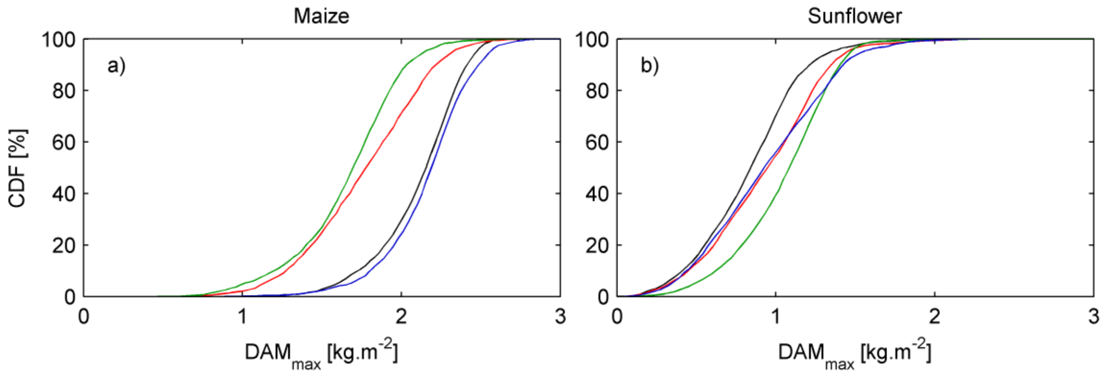

Figure 16: Cumulative distribution function (CDF) of maximum dry aboveground mass (DAM_{max}) simulated for maize (a) and sunflower (b) in 2006 (black), 2007 (red), 2008 (green) and 2009 (blue) over the entire Formosat-2 footprint. The amount of data used is shown in Fig. 11 a and b.

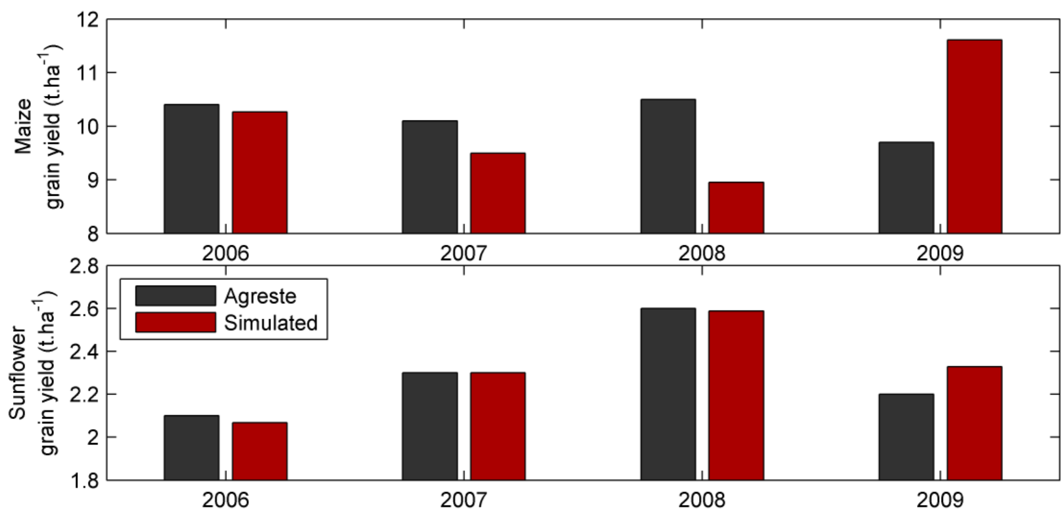

Figure 17: Comparison of the four-year grain yield (in t.ha^{-1}) obtained from Agreste (2011) for the French department of Haute-Garonne and the yield simulated for the study area.

Tables

Table 1: In situ measurements data description, including crop type, year of in situ measurements, and number of data collected for GAI, FAPAR and DAM. The sampling scheme is given in the two last columns: ESU (with the number of sampled field under bracket) or transect (Lamothe and Auradé). GAI and FAPAR were estimated from hemispherical photographs and DAM was estimated from destructive measurements.

<table>
<tr><th>Crop type</th><th>Year</th><th>GAI / FAPAR</th><th>DAM</th></tr>
<tr><td rowspan="4">Maize</td><td>2006</td><td rowspan="4">ESU (3): 23</td><td>Lamothe: 6</td></tr>
<tr><td rowspan="2">2008</td><td>ESU (1): 9</td></tr>
<tr><td>Lamothe: 6</td></tr>
<tr><td>2009</td><td>ESU (5): 5</td></tr>
<tr><td rowspan="3">Sunflower</td><td>2007</td><td rowspan="3">ESU (2): 19</td><td>Auradé: 7</td></tr>
<tr><td>2008</td><td>ESU (2): 9</td></tr>
<tr><td>2009</td><td>ESU (2): 2</td></tr>
</table>

Table 2: List of the SAFY input parameters and initial values estimated from the literature for ε_C, T_{min}, T_{opt}, T_{max}, β and DAM_0, from measurements of K_{ext} and SLA from the calibration procedure for the crop specific (Pl_a, Pl_b, Rs, Stt) and field specific (D_0, ELUE) parameters.

Parameter type and name	Notation	Unit	Range	Grain Maize	Silage Maize	Sunflower
Constant (literature)						
Climatic efficiency	ε_C	-		0.48*	0.48*	0.48*
Initial dry aboveground mass	DAM_0	$g.m^{-2}$		4.2	4.2	6.9
Temperature for growth [Minimal, Optimal, Maximal]	T_{min}, T_{opt}, T_{max}	°C		[8 30 45]$^+$	[8 30 45]$^+$	[8 28.5 42]‡
Polynomial degree	β	-		2	2	3
Constant (measured)						
Light-interception coefficient	K_{ext}	-		0.63	0.63	0.63
Specific leaf area	SLA	$m^2.g^{-1}$		0.024	0.024	0.012
Calibrated (Crop-specific)						
Partition-to-leaf function: par a	Pl_a	-	[0.05 0.5]	0.35	0.34	0.13
Partition-to-leaf function: par b	Pl_b	-	[10^{-5} 10^{-2}]	0.0026	0.0027	0.0033
Rate of senescence	Rs	°C.day	[0 10^5]	7410	457	5787
Temperature sum for senescence	Stt	°C	[0 2000]	1028	1002	713
Calibrated (Field-specific)						
Day of plant emergence	D_0	DoY	[90 250]			
Effective light-use efficiency	ELUE	$g.MJ^{-1}$	[0.5 6]			

* Varlet-Grancher et al. (1982)

$^+$ Drouet and Pages (2003)

‡ Stics website (http://www.avignon.inra.fr/agroclim_stics/)

Table 3: Statistics derived from the comparison of the SAFY simulated and the measured dry aboveground mass (DAM).

	Maize	Sunflower	All crops
N	26	18	44
RMSE (kg.m^{-2}	0.252	0.145	0.215
RRMSE (%)	24.67	39.11	28.44
Bias (kg.m^{-2})	-0.070	0.049	-0.021
r^2	0.91	0.78	0.92

Appendix 1: Overview of the SAFY model.

The simple algorithm for yield estimates (SAFY, Duchemin et al. 2008a) is a daily time-step model that simulates time series of leaf area index (LAI) and dry aerial mass (DAM) from the air temperature (Ta) and the global incoming radiation (Rg). The simulations begin on the plant emergence day (D_0). D_0 depends on agricultural practices (in particular sowing date and depth) and on the pedoclimatic conditions and constrains the phase of the LAI time course.

Daily DAM production (Δ_{DAM}) is calculated through the approach of Monteith (1977, Eq. 2) using an effective light-use efficiency (ELUE), a daily temperature stress factor (F_T) and the daily photosynthetically active radiation absorbed by plants (APAR). The ELUE expresses the conversion of the APAR into DAM. It is supposed to account for all agri-environmental stresses, such as water and nitrogen supplies, except for temperature. It constrains the amplitude of the GAI time course. The temperature stress function is a classical Polynomial (Eq. 3) of β Degree defined by an optimal daily mean air temperature (T_{opt}) for maximum crop functioning and two extreme temperatures (T_{min} and T_{max}) beyond which the plant growth stops (after Brisson et al. 2003). The APAR (Eq. 4) is computed using the daily incoming global radiation (Rg), the climatic efficiency (ε_C) and the fraction of the photosynthetically active portion of solar radiation absorbed by green plants (FAPAR). In the SAFY model, the FAPAR is estimated using Beer's law (Eq. 5), where k_{ext} defines the light-extinction coefficient (Monsi and Saeki 1953).

$$\Delta_{DAM} = ELUE \times F_T(Ta) \times APAR \qquad (2)$$

$$\begin{cases} F_T(Ta) = 1 - \left(\dfrac{T_{opt} - Ta}{T_{opt} - T_{\min}} \right)^{\beta} & if \qquad T_{\min} < Ta < T_{opt} \\ F_T(Ta) = 1 - \left(\dfrac{T_{opt} - Ta}{T_{opt} - T_{\max}} \right)^{\beta} & if \qquad T_{\max} > Ta > T_{opt} \\ F_T(Ta) = 0 & if \quad Ta < T_{\min} \quad OR \quad Ta > T_{\max} \end{cases} \tag{3}$$

$$APAR = FAPAR \times \varepsilon_C \times Rg \tag{4}$$

$$FAPAR = 1 - e^{-k_{ext} \times LAI} \tag{5}$$

During plant growth, a fraction of the daily plant DAM production is partitioned to the dry leaf biomass. This fraction is calculated using the partition-to-leaf function Pl (Eq. 6, after Maas 1993), which varies from 0 to 1. Pl is a function of the daily air temperature cumulated from plant emergence (SMT: sum of temperature, Eq. 7) and two parameters: Pl_a and Pl_b. It should be noted that (1 – Pl_a) defines the rate of biomass allocation to leaves at plant emergence. Daily leaf mass production (Δ_{DAM} × Pl) is converted into daily leaf area growth ($\Delta^+_{\mathbf{LAI}}$) based on the specific leaf area (SLA, Eq. 8). Leaf senescence (Δ^-_{LAI}) begins when the SMT reaches a given threshold (Stt, sum of temperature for senescence). It is modelled by a function (Eq. 9) based on the rate of senescence coefficient (Rs). The LAI is updated from the balance of Δ^+_{LAI} and Δ^-_{LAI} (Eq. 10).

$$Pl = 1 - Pl_a \times e^{Pl_b \times SMT} \tag{6}$$

$$SMT = \sum_{D_0}^{t} \left(Ta_t - T_{\min} \right) \cdot dt \tag{7}$$

If Pl>0, $\Delta_{LAI}^{+} = \Delta_{DAM} \times Pl \times SLA$ (8)

If SMT>Stt, $\Delta_{LAI}^{-} = LAI \times \frac{SMT - Stt}{Rs}$ (9)

$$LAI_{t} = LAI_{t-1} + \Delta_{LAI}^{+} - \Delta_{LAI}^{-} \quad (10)$$